PCCP

Accepted Manuscript

ROYAL SOCIETY OF CHEMISTRY

www.rsc.org/pccp

Comparison of Direct Dynamics Simulations with Different Electronic Structure Methods. $F^- + CH_3I$ with MP2 and DFT/B97-1

Rui Sun,[a] Collin J. Davda,[a,b] Jiaxu Zhang[c] and William L. Hase[a,*]

[a]Department of Chemistry and Biochemistry
Texas Tech University,
Lubbock, Texas 79409-1061

[b]Trinity Valley School
Fort Worth, Texas 76132-4553

[c]Institute of Theoretical and Simulation Chemistry
Academy of Fundamental and Interdisciplinary Sciences
Harbin Institute of Technology
Harbin 150080, P. R. China

Abstract

In previous work, ion imaging experiments and direct chemical dynamics simulations with DFT/B97-1 were performed to study the atomic-level dynamics of the $F^- + CH_3I \rightarrow FCH_3 + I^-$ S_N2 nucleophilic substitution reaction at different collision energies. Overall, the simulations are in quite good agreement with experiment at the low collision energy of 0.32 eV, however there are differences between experiment and simulation at the high collision energy of 1.53 eV. A recent CCSD(T) study of the potential energy surface for the $F^- + CH_3I \rightarrow FCH_3 + I^-$ S_N2 reaction shows that it has both a traditional C_{3v} and a hydrogen-bond entrance channel. They are represented by MP2 but not by B97-1, which has only the latter channel. On the other hand, B97-1 gives a reaction exothermicity in excellent agreement with experiment, while MP2 is in error by 24.3 kJ/mol. In the work presented here, direct dynamics simulations using MP2/aug-cc-pvdz/ECP/d were performed for the $F^- + CH_3I \rightarrow FCH_3 + I^-$ reaction at a 1.53 eV collision energy. The same direct rebound and stripping and indirect atomistic reaction mechanisms are found in the B97-1 and MP2 simulations. Both the B97-1 and MP2 simulations agree with the experimental fraction of the available product energy partitioned to CH_3F internal energy, i.e. f_{int} = 0.59 ± 0.08. However, the MP2 f_{int} distribution is broader and in better agreement with experiment than B97-1. The two simulations methods give the same product energy partitioning for the stripping mechanism, but different partitionings for the rebound and indirect mechanisms. Compared to experiment, the principal difference between the B97-1 and MP2 results is the differential cross section which is nearly isotropic for B97-1. For MP2 backward scattering is more important than forward, as found in the experiments. Though there is no overall barrier for the reaction, B97-1 gives a reaction cross section appreciably larger than that for MP2, i.e. 8.6 ± 2.2 $Å^2$ versus 1.8 ± 0.3 $Å^2$. For B97-1 59% of the reaction consists of indirect mechanisms, while for MP2 the indirect mechanisms only comprise 11% of the reaction. The experimental differential cross section is more consistent with the atomistic mechanisms for MP2 than for B97-1.

I. Introduction

Study of gas-phase $X^- + CH_3Y \rightarrow CH_3X + Y^-$ S_N2 reactions is of particular interest to many experimental and theoretical chemists, for they are paradigm reactions in physical organic chemistry.[1-10] The traditional potential energy surface (PES) for this reaction has an ion-dipole X^----CH_3Y pre-reaction complex, a $[X--CH_3--Y]^-$ central barrier, and an ion-dipole XCH_3---Y^- post-reaction complex, all of C_{3v} symmetry.[10] Non-traditional (non-C_{3v} symmetry) PESs are often important; e.g. the $OH^- + CH_3F$ S_N2 reaction with a CH_3OH---F^- post-reaction complex in which F^- is hydrogen-bonded to the –OH moiety,[11] and the $F^- + CH_3I$ reaction with a hydrogen-bonded F^----HCH_2I pre-reaction complex.[12]

In previous work Zhang *et al.*[12] investigated the PES for the $F^- + CH_3I \rightarrow FCH_3 + I^-$ S_N2 reaction with different electronic structure theories and basis sets. Of particular interest is that MP2[13] and DFT[14] give different entrance-channel PESs for this reaction, as shown in Figure 1. For the DFT/B97-1 PES there are only a hydrogen-bonded F^----HCH_2I pre-reaction complex and a hydrogen-bonded $[F--HCH_2--I]^-$ transition state (TS). In contrast, the MP2 PES has these stationary point structures as well as the traditional F^----CH_3I ion-dipole complex and $[F--CH_3--I]^-$ TS, both with C_{3v} symmetry. The DFT functionals OPBE,[15] OLYP,[16] HCTH407,[17] and BhandH,[18] give PESs similar to the B97-1 PES in Figure 1, and only BhandH with a triple-zeta basis set gives traditional entrance-channel C_{3v} stationary points similar to those for the MP2 PES.[12]

The DFT/B97-1/ECP/d level of theory was chosen for the previous direct dynamics simulations[19,20] of the $F^- + CH_3I$ reaction, since it gives a heat of reaction in excellent agreement with experiment. The simulations were performed at collision energies at 0.32 and 1.53 eV, and overall quite good agreement was found with experiment; e.g. the experimental and simulation average fractions of product energy partitioning are statistically the same. However, for the higher energy 1.53 eV collisions differences were found between the experimental and simulation dynamics.[20] The internal energy distribution of the CH_3F product is narrower in the simulations than in the experiments, and the product scattering angle distribution is nearly isotropic in the simulations, but has an important backward scattering component in the experiments.

Recently, Sun *et al.*[21] performed CCSD(T)[22] single point optimization calculations with different basis sets to assess the accuracy of the MP2 and DFT PESs for the $F^- + CH_3I \rightarrow FCH_3$

+ I^- entrance-channel stationary points. Similar to the MP2 PES, both the hydrogen-bonded and traditional C_{3v} stationary points were found for the CCSD(T) PES with all basis sets considered. The energetics for the CCSD(T)/PP/t PES are depicted in Figure 1 and the other basis sets give a similar result; i.e. all of the basis set used for the CCSD(T) calculations are described below as well as in references 12 and 21. These CCSD(T) calculations strongly suggest that the $F^- + CH_3I$ entrance-channel has C_{3v} stationary points as found for the MP2 PES, which are absent in PESs determined from all of the DFT calculations except one.[12]

In the work presented here MP2/ECP/d direct dynamics simulations were performed to investigate the possibility that the differences in the MP2 and B97-1 PESs affect the reaction dynamics. Interestingly, B97-1 gives reactive scattering dynamics at 0.32 eV which are in good agreement with experiment and the differences are found at the higher collision energy of 1.53 eV.[19, 20] Accordingly, the MP2 simulations were performed for this latter energy to compare the results with experimental data as well as the previous simulations using B97-1/ECP/d.[20] Section II describes the computational methodology for both the *ab initio* calculations and direct dynamics simulations, and the results of the simulations are presented in Section III. Differences between the MP2 and DFT simulation results are discussed in Section IV. The article ends with a Summary in Section V.

II. Computational Methodology

A. *Ab initio* calculations

The MP2/ECP/d method was used for the direct dynamics simulations. Detailed discussions of different electronic structure calculations for the $F^- + CH_3I \rightarrow FCH_3 + I^-$ PES are discussed elsewhere[12, 21] and briefly presented here. The ECP/d basis set is a combination of: the Wadt and Hay effective core potential (ECP)[23] for the core electrons; Dunning and Woon's aug-cc-pVDZ basis set[24, 25] for the C, H, and F atoms; and for iodine a 3s, 3p basis set for the valence electrons, augmented by a d-polarization function with a 0.262 exponent, and s, p, and d diffuse functions with exponents of 0.034, 0.039, and 0.0873.[26] The PP/t basis set consists of the aug-cc-pVTZ basis set[24, 25] for the C, H, and F atoms, and Peterson's aug-cc-pVTZ basis set, with a pseudopotential (PP) for iodine.[27]

Similar to the CCSD(T)/PP/t PES shown in Figure 1, the MP2/ECP/d PES has both the traditional C_{3v} and hydrogen-bonded entrance channels, with the respective $[F\text{--}CH_3\text{--}I]^-$ and [F--

HCH_2--I]$^-$ TSs. Intrinsic reaction coordinate (IRC)[28] calculations were performed to understand the connectivity of the C_{3v} and hydrogen-bonded stationary points for the MP2 PES.[12] The hydrogen-bonded TS is connected with both the hydrogen-bonded and C_{3v} pre-reaction complexes. The C_{3v} TS is connected with the C_{3v} pre- and post-reaction complexes.

For the MP2/ECP/d PES, the classical potential energy difference between the F^----CH_3I pre-reaction complex and [F--CH_3--I]$^-$ TS for the C_{3v} pathway is 2.9 kJ/mol, and 13.0 kJ/mol between the F^----HCH_2I pre-reaction complex and [F--HCH_2--I]$^-$ TS for the hydrogen-bonded pathway. The corresponding CCSD(T)/PP/t energies are 1.9 kJ/mol and 12.0 kJ/mol. The respective classical potential energy release values from the F^- + CH_3I separated reactants to the F^----CH_3I C_{3v} complex and to the F^----HCH_2I hydrogen-bonded complex are 68.2 and 79.1 kJ/mol for MP2/ECP/d, compared to 71.5 and 81.4 kJ/mol for CCSD(T)/PP/t. Stationary point geometries are given in Table 2 of reference 21, and MP2/ECP/d gives structures very similar to those for CCSD(T)/PP/t. As a result of these comparisons between CCSD(T) and MP2, MP2/ECP/d was chosen as the electronic structure method for direct dynamics simulations to investigate the effect of the "additional" C_{3v} entrance channel pathway compared to the previous DFT simulations.[19,20]

The energies in Figure 1 are classical potential energies and, if harmonic zero-point energy (zpe) is included, the energies (kJ/mol) for the stationary points with respect to F^- + CH_3I are: F^----HCH_2I, -79.5; [F--HCH_2--I]$^-$, -66.1; F^----CH_3I, -67.4; [F--CH_3--I]$^-$, -64.4; FCH_3---I^-, -200.4; and FCH_3 + I^-, -164.8. These energies with zpe included are similar to the classical potential energies, except for the post-reaction complex and products. For these two stationary points, the CH_3F vibrational frequencies are substantially different from those for the reactant CH_3I.

B. Direct dynamics simulations

Classical trajectory simulations have been widely used to study chemical dynamics since the early 1960's.[29] They provide important atomic-level information such as reaction pathways,[30] rate constants,[31] and intramolecular vibrational energy redistribution (IVR) rates.[32] A broadly applicable approach for performing these simulations is Born-Oppenheimer direct dynamics[33-35] for which the potential energy and its gradient, needed to numerically solve the classical equations of motion, are obtained directly from an electronic structure theory. An enhancement in the simulation efficiency is to use the molecular orbitals (MOs) obtained from the previous

integration step to initiate the self-consistent field[36] (SCF) procedure for the current integration step. This approach ensures the trajectory remains on the same adiabatic electronic state, since the MOs for the previous step are expected to have the same character as those for the current integration step. The direct dynamics simulations presented here were performed with the VENUS/NWChem[37] software package, which has tight coupling between the classical dynamics simulation code VENUS[38,39] and the electronic structure code NWChem.[40]

C. Trajectory initial conditions and calculations

For the best accuracy and computational cost, the trajectory integrations were performed with the velocity-Verlet[41] method using a time step is 0.2 fs. The trajectories were integrated for a maximum time of 5 ps, or until the distance between C-I or C-F exceeded 15 Å, which was considered to be formation of products or reactants, respectively. Initial conditions for the simulations were chosen to be identical with the experiments to compare simulation and experiment. Quasiclassical sampling[42] was used to select initial conditions for CH_3I with 360 K and 75 K vibrational and rotational temperatures, respectively. The CH_3I molecule was randomly rotated about its Euler angles. The $F^- + CH_3I$ collision energy is fixed at 1.53 eV with an initial separation of 15 Å. Different impact parameters were chosen for the collision as described below.

Before presenting the results of the simulations, it is important to assess the accuracy of classical dynamics for the $F^- + CH_3I \rightarrow CH_3F + I^-$ S_N2 reaction. Classical dynamics do not preserve zpe constraints,[43] and bimolecular[44,45] and unimolecular[46] reactions can occur classically without zpe in the modes orthogonal to the reaction coordinate as the reactive system passes the TS. Thus, if tunneling is unimportant, the classical threshold for reaction will be less than that for quantum dynamics. For intramolecular vibrational energy redistribution (IVR),[32] classical dynamics may allow zpe to unphysically flow from a mode and enhance the rate of IVR.[47,48]

The neglect of zpe constraints in classical dynamics becomes important when the energy of the reactive system is in only slight excess of its zero point energy. Fortunately, as a result of the high collision energy of 1.53 eV and the large exothermicity in forming the pre-reaction complex and reaction products, problems with zpe are unexpected for the $F^- + CH_3I \rightarrow CH_3F + I^-$ S_N2 reaction. The reactive system is expected to have zpe when crossing the TS, separating the pre-reaction complex and products, and when forming the products. Thus, classical dynamics is

expected to be accurate for the $F^- + CH_3I \rightarrow CH_3F + I^-$ S_N2 reaction at a collision energy of 1.53 eV, and any differences between the classical dynamics simulations and experiment are expected to result from shortcomings in the PES.

III. MP2 Simulation Results

A. Microscopic reaction mechanisms, reaction probabilities, and cross sections

The reaction dynamics were studied by calculating ensembles of trajectories at fixed values of impact parameter *b*. To identify the largest impact parameter at which reaction occurs, b_{max}, 200 trajectories were calculated for each *b* of 4.75, 5.00, 5.25, 5.50, 5.75, 6.00 Å. For this range of *b*, reaction was observed at only *b* of 4.75Å and not at the higher *b*. Therefore, 4.75 Å was identified as b_{max} and subsequent trajectories were sampled with *b* less than this b_{max}, and 500 trajectories were calculated for each of *b* of 0, 1, 2, 3, 4, and 4.75 Å. Two reaction pathways were observed, i.e. S_N2 nucleophilic substitution $F^- + CH_3I \rightarrow FCH_3 + I^-$ and proton transfer $F^- + CH_3I \rightarrow HF + CH_2I^-$. The research discussed here focuses on the S_N2 reaction and the dynamics of proton transfer will be considered in the future.

The S_N2 reaction probability versus impact parameter is shown in Figure 2. Even though the reaction has no overall barrier, the simulations still predict a very low reaction probability, i.e. less than 12% for each impact parameter, which decreases as the impact parameter increases. Similar to what has been observed for other S_N2 reactions,[19,20,49] the reaction occurs by two direct atomic-level mechanisms, i.e. rebound and stripping, and different types of indirect mechanisms. For the direct rebound mechanism F^- directly attacks the backside of CH_3I, rebounds backward off the massive I-atom, and forms a highly excited C-F bond in CH_3F molecule. The stripping direct reaction mechanism occurs when F^- approaches the side of the methyl iodide molecule and strips the methyl group away from the I-atom, with CH_3F scattering in the forward direction. This reaction mechanism gives the newly formed CH_3F molecule an increased amount of rotational energy. Depictions of the rebound and stripping mechanisms are given in a previous article describing $F^- + CH_3I$ S_N2 dynamics.[19]

The indirect reaction is more complicated and occurs by multiple mechanisms including formation of the pre-reaction complex (A) or post-reaction complex (B), the roundabout mechanism (Ra),[50] barrier recrossing (br),[51,52] and combinations of these processes. For complex formation, one or both of the pre-reaction complexes F^----CH_3I and F^----HCH_2I and/or post-

reaction complex FCH_3---I^- have multiple vibrations between the anion and the molecular moiety, resulting in a lifetime that is observable in the atomic animations. Barrier recrossing was first observed for S_N2 reactions in $Cl^- + CH_3Cl$ central barrier dynamics.[51] For the roundabout mechanism, F^- first strikes the CH_3 group on its side, causing it to rotate one or more times around the massive I atom. Then, after one or more CH_3 revolutions, F^- attacks the C atom backside and directly displaces I^-. This reaction mechanism has been discussed in detail previously.[50] Percentages for the different indirect mechanisms are complex formation (42%), barrier recrossing (32%), roundabout (16%), and barrier recrossing + complex formation (10%).

As reported for other S_N2 reactions[19,20,49] and shown in Figure 2, the probabilities of the atomistic mechanisms are heavily dependent on *b*. Direct rebound is the most likely mechanism at small *b*, for which the incoming fluoride ion attacks carbon backside. Direct stripping replaces direct rebound as the most probable mechanism at larger *b*. The probability of the indirect mechanism decreases near linearly as *b* increases. The reaction cross section σ_r is obtained by integrating the reaction probability versus *b*, $P_r(b)$, over *b*; i.e. $\sigma_r = 2\pi \int P_r(b) b db$. The total reaction cross section is 1.8 ± 0.3 Å^2, and those for the direct rebound, direct stripping, and indirect mechanisms are 0.8 ± 0.3 Å^2, 0.8 ± 0.2 Å^2, 0.2 ± 0.06 Å^2, respectively. The rebound, stripping, and indirect percentages of the reaction are 46, 43, and 11 %, respectively.

B. Product energy partitioning

The average I^- + CH_3F product energy partitioning for the current MP2/ECP/d simulations are given in Table 1. The overall fraction partitioned to CH_3F rotation + vibration is 0.66 ± 0.01 from MP2/ECP/d, statistically the same as the experimental result of 0.59 ± 0.08.

Figure 3 presents the distribution of the CH_3F internal energy, obtained from the MP2 simulations, which is compared with the experimental distribution. The two distributions are similar, in that both have the same upper bound of ~3.4 eV.[20] Both distributions have the same most probable internal energy of 2.4 eV and also similar shapes in the vicinity of the distributions' peaks. The experimental data contains a more diffuse lower bound in the distribution, due to the finite energy resolution,[20] which is not present in the MP2 simulations. Overall the MP2/ECP/d internal energy distribution for CH_3F is in agreement with experiment.

C. Center-of-mass velocity scattering angle

The scattering angle θ, between the reactant and product ion relative velocity vectors,[50] was calculated for each reactive trajectory. The resulting distribution of this angle includes all

values within the 2π solid angle, whose area is proportional to sinθ, and a comparison may be made with experiment.[20,50] The experiments only determine the relative intensity of the scattering versus θ,[20,50] and the experimental and simulation relative scattering intensities are compared here.

Figure 4 presents the histogram of the cosine of the scattering angle θ for the total S_N2 reaction and Figure 5 presents the histograms for the rebound, stripping, and indirect atomistic mechanisms. The direct rebound mechanism leads to a backward scattering with cosθ negative, as the CH_3F product fluorine bounces off the much more massive iodine atom. Though the direct stripping mechanism leads to forward scattering with cosθ positive, a large faction of the direct stripping trajectories have scattering with the cosine value close to zero (see previous discussion in references 19 and 20). Isotropic scattering is observed for the combined indirect mechanisms, as found in previous studies.[19,20,49] For the total reaction, there is good agreement between the experimental scattering angle distribution[20] and the scattering distribution determined from the MP2 simulations, particularly for the forward and backward regions. However, the simulations predict a large portion of the scattering with cosθ close to zero, which is absent in the experiments.[20] It is of interest that almost all of the "sideways" scattered trajectories, with cosθ close to zero, are from the ensemble with an impact parameter *b* of 3 Å, with very few coming from the ensembles with *b* of 1 and 2 Å. Thus, it is possible that this sideways scattering would not be as pronounced if *b* was sampled continuously between 0 and b_{max} for the simulations.[42] Nevertheless, the MP2 scattering angle distribution is dominated by backward scattering and in overall agreement with experiment.

IV. Comparison of MP2 and DFT/B97-1 Direct Dynamics

In the following, the MP2 simulation results reported above are compared with the previous B97-1 results.[19,20]

A. Reaction probabilities and cross sections

The MP2 and B97-1 total S_N2 reaction probabilities versus impact parameter, $P_r(b)$, are compared in Figure 2. The B97-1 $P_r(b)$ are approximately a factor of two larger than the MP2 values and, in addition, $P_r(b)$ extends to ~6 Å for B97-1 but only to ~5 Å for MP2. As a result, the B97-1 S_N2 reaction cross section is appreciably higher than the MP2 value and is 8.6 ± 2.2 $Å^2$, as compared to 1.8 ± 0.3 $Å^2$ for MP2. This difference in the MP2 and B97-1 reactive cross

sections probably arises from multiple factors. One is the broader range of impact parameters leading to reaction for the B97-1 dynamics. Another is that for MP2 the TS connecting the pre-reaction complex to the products is ~ 10 kJ/mol higher in energy (see Figure 1).

As shown in Figure 2, the MP2 and B97-1 dynamics have the same direct rebound, direct stripping, and indirect atomistic mechanisms. The overall characteristics of the MP2 and B97-1 $P_r(b)$ are similar for the rebound and stripping mechanisms, with the proviso that the rebound $P_r(b)$ are larger for the B97-1 calculations. The striking difference between the MP2 and B97-1 dynamics is for the indirect mechanism, whose B97-1 probability peaks at large impact parameters. For the b = 0-3 Å range, the $P_r(b)$ for MP2 and B97-1 are similar, but for the larger b B97-1 has a much higher probability for the indirect mechanism. The B97-1 cross sections for the rebound, stripping, and indirect mechanisms are 2.5 ± 0.7, 1.0 ± 0.3, and 5.1 ± 1.7 Å^2, respectively, which give respective probabilities of 29, 12, and 59 %, respectively. The MP2 cross sections for the rebound, stripping, and indirect mechanisms are 0.8 ± 0.3 Å^2, 0.8 ± 0.2 Å^2, and 0.2 ± 0.06 Å^2, respectively, resulting in respective percentages of 46, 43, and 11 %. Thus, the indirect mechanism is dominant (59%) for the B97-1 dynamics, but a minor contributor (11%) for MP2. The B97-1 cross section for the rebound mechanism is four times larger than the MP2 value, while the B97-1 and MP2 cross sections are the same for the stripping mechanism.

B. Product energy partitioning

The average product energy partitioning fractions for the DFT/B97-1 and MP2 simulations are summarized in Table 1. The overall DFT/97-1 and MP2 fractions partitioned to CH_3F internal excitation, f_{int}, are 0.63 ± 0.04 and 0.66 ± 0.01, respectively, and statistically the same as the experimental result of 0.59 ± 0.08. In addition, the partitionings to f_{rot}, f_{vib}, and f_{rel} are also the same for B97-1 and MP2.

Differences in the energy partitioning are apparent for the atomic-level rebound and indirect mechanisms. The B97-1 and MP2 energy partitionings are similar for the stripping mechanism. For the rebound mechanism, B97-1 preferentially transfers energy to product relative translation (0.54), while the majority of the transfer is to CH_3F vibration (0.56) with MP2. Correspondingly, f_{int} is 0.46 for B97-1 and 0.63 for MP2. For the indirect reaction, f_{rel} for MP2 is one-half that for B97-1. As a result, f_{int} is 0.85 and 0.69 for MP2 and B97-1, respectively.

The CH_3F internal energy distributions, from the B97-1 and MP2 simulations, are compared in Figure 3. Both B97-1 and MP2 have the same high energy cut-off, but overestimate

the distribution in the region of approximately 1.5-2.5 eV. Both B97-1 and MP2 do not capture the low energy region of the distribution as compared to experiment.[20] However, there is some experimental uncertainty for this region due to diffuseness in the data and, resulting, finite energy resolution.[20] The most probable energy of 2.4 eV from the MP2 simulations is similar but slightly larger than the B97-1 value of 2.2 eV. Overall, the MP2 internal energy distribution is broader and in better agreement with experiment than B97-1.

C. Center-of- mass velocity scattering angle

The MP2 and B97-1 center-of-mass velocity scattering angle distributions are given in Figure 4, where they are compared with experiment. Experiment is dominated by backward scattering, but B97-1 predicts almost isotropic scattering. The MP2 scattering angle distribution agrees well with experiment, except for a surprisingly large probability of sideways scattering, that is discussed in Section III.C. Overall, the MP2 simulations reproduce the backward scattering observed in the experiments. This is a result of less indirect reaction in MP2 as compared to the B97-1 simulations and the, resulting, more important rebound mechanism for the MP2 simulations.

The MP2 velocity scattering angle distributions for the rebound, stripping, and indirect mechanisms are compared in Figure 5, and their characteristics are similar to what was found for the previous B97-1 simulations. Rebound is backward scattering, stripping forward, and indirect overall isotropic. What is different between the MP2 and B97-1 scattering is the sideways component in the MP2 stripping, which is not present for B97-1.

V. Summary

In the work presented here MP2/ECP/d direct dynamics for the $F^- + CH_3I \rightarrow CH_3F + I^-$ S_N2 reaction, at a collision energy of 1.53 eV, are compared with those presented previously using the B97-1/ECP/d method.[19,20] There are differences between the B97-1 and experimental results for this collision energy. Comparisons are often made between different electronic structure methods in calculating stationary point properties such as structures, vibrational frequencies, and energies, and it is important to understand how the reaction dynamics depend on the level of electronic structure theory used in direct dynamics simulations. The work presented here addresses this subject.

There are differences in the entrance channel for the MP2 and B97-1 PESs.[12] As shown in Figure 1, for B97-1 there is only the hydrogen-bonded pathway, while for MP2 there is this pathway and the traditional C_{3v} pathway. The MP2 PES agrees with higher level CCSD(T) calculations,[21] which is expected to be accurate. The effect of such an inaccuracy in the reaction pathways for the B97-1 PES might be expected to be most pronounced at low energy. However, interestingly, B97-1 gives overall dynamics which agree with experiment at the low collision energy of 0.32 eV.[19,20] It is at the higher collision energy of 1.53 eV where there are differences between the B97-1 dynamics and experiment. This is the energy considered here.

MP2 and B97-1 give the same atomistic direct rebound, direct stripping, and indirect atomistic mechanisms for the $F^- + CH_3I \rightarrow CH_3F + I^-$ S_N2 reaction, but these theories differ in the relative importance of these mechanisms and in the total reaction cross section. The major difference for the atomistic mechanisms is that B97-1 predicts that 59% of the reaction is indirect, while only 11% for MP2. In addition, the rebound mechanism is more important for the MP2 dynamics. A property which conceivably could be determined by experiment is the S_N2 reaction cross section, for which the B97-1 and MP2 values are 8.6 ± 2.2 and 1.8 ± 0.3 $Å^2$, respectively. Experiment could identify which is more accurate, which may provide insight to whether MP2 or B97-1 more accurately describes the atomic-level mechanisms. It is noteworthy that the experimental scattering is characterized by nearly equal isotropic and backward scattered components, indicating an appreciable indirect component in the scattering dynamics.[20]

Both B97-1 and MP2 give an average energy partitioning to CH_3F internal energy which is in agreement with experiment. However, the MP2 distribution for this energy is in somewhat better agreement with experiment than found from the B97-1 simulations, but there is some uncertainty in the exact form of the experimental distribution.[20] The stripping mechanism gives similar energy partitioning for the MP2 and B97-1 simulations, but the energy partitioning is different for the rebound and indirect mechanisms. For MP2 the majority of the rebound energy partitioning is to CH_3F vibration, but for B97-1 it is to relative translation. For the indirect mechanism, MP2 partitions 0.85 of the available energy to CH_3F internal energy and, in contrast, this fraction is 0.69 for B97-1. These are interesting differences in the atomistic product energy partitioning, which are difficult to determine experimentally. For example, the rebound mechanism has backward scattering, but this scattering is convoluted with that for the indirect mechanism which also has a backward component.

The MP2 differential cross section is in much better agreement with experiment than found from the B97-1 simulations. There is a large backward (i.e. rebound) component in the experimental scattering and B97-1 does not give this. Instead, these simulations give a near isotropic scattering distribution.

The above comparisons between experiment and the MP2 and B97-1 simulations, at a collision energy of 1.53 eV, suggest the former may be more accurate. However, more experimental information is needed, e.g. the S_N2 reaction cross section. For the 12-dimensional 6-atom $F^- + CH_3I \rightarrow CH_3F + I^-$ reaction, it is difficult to quantify which differences in the MP2 and B97-1 PESs affect the 1.53 eV reaction dynamics. The B97-1 PES has a classical heat of reaction of -195.4 kJ/mol which is in excellent agreement with the experimental value of -196.7 kJ/mol, while that for MP2 is -172.4 kJ/mol and in error by 24.3 kJ/mol.[21] In addition, direct dynamics simulations for the $OH^- + CH_3I$ reaction, with B97-1, give rate constants in excellent agreement with experiment.[53] On the other hand, CCSD(T) calculations[21] indicate that MP2 more accurately describes the entrance channel reaction paths for the S_N2 reaction. The MP2 barrier, for the TS connecting the pre-reaction complex with products, is ~ 10 kJ/mol higher than the B97-1 barrier. However, the reaction exothermicity, entrance channel reaction paths, and TS barrier for pre-reaction complex to products are just signatures of the PES, and may only make minor contributions to the dynamics for the high energy 1.53 eV reaction. In inspecting the trajectories, it is found that 55 % of the reaction follows an indirect mechanism with B97-1, but only 11 % with MP2. Such differences, as well as the ~ 4 times larger reaction cross section with B97-1, most likely result from high energy features of the PES. More work needs to be done to determine which electronic structure theories, and their PES properties, give accurate dynamics for the $F^- + CH_3I \rightarrow CH_3F + I^-$ S_N2 reaction at both low and high energies. Overall, this work has illustrated the utility of direct dynamics simulations for assessing the accuracy of electronic structure theories and their PESs. Additional studies like the one presented here are important.

Acknowledgements

The direct dynamics simulations reported here are based upon work supported by the Robert A. Welch Foundation under Grant No. D-0005. Support was also provided by the High-Performance Computing Center (HPCC) at Texas Tech University, under the direction of Philip W. Smith, the Texas Advanced Computing Center (TACC) at the University of Texas, Austin,

and the TTU Department of Chemistry & Biochemistry cluster Robinson, whose purchase was funded by the National Science Foundation under the CRIF-MU Grant No. CHE-0840493. The authors wish to acknowledge the Welch Summer Scholar Program which supported the summer research of Collin Davda. Jiaxu Zhang acknowledges the Fundamental Research Funds for the Central Universities, China (AUGA5710012114) for support of his research. The authors also wish to acknowledge important collaborations with the Roland Wester group regarding S_N2 reaction dynamics.

References

1. Lieder, C. A.; Brauman, J. I. *J. Am. Chem. Soc.* **1974**, *96*, 4028-4030
2. Olmstead, W. N.; Brauman, J. I. *J. Am. Chem. Soc.* **1977**, *99*, 4219-4228
3. Hase, W. L. *Science* **1994**, *266*, 998-1002
4. Peslherbe, G. H.; Wang, H.; Hase, W. L. *J. Am. Chem. Soc.* **1996**, *118*, 2257-2266
5. Wang, H.; Hase, W. L. *J. Am. Chem. Soc.* **1997**, *119*, 3093-3102
6. Chabinyc, M. L.; Craig, S. L.; Regan, C. K.; Brauman, J. I. *Science*, **1998**, *279*, 1882-1886
7. Gonzales, J. M.; Cox, R. S., III.; Brown, S. T.; Allen, W. D.; Schaefer, H. F., III. *J. Phys. Chem. A.* **2001**, *105*, 11327-11346
8. Laerdahl, J. K.; Uggerud, E. *Int. J. Mass Spectrom.* **2002**, *214*, 277-314
9. Sun, L.; Song, K.; Hase, W. L. *Science* **2002**, *296*, 875-878
10. Manikandan, P.; Zhang, J.; Hase, W. L. *J. Phys. Chem. A.* **2012**, *116*, 3061-3080
11. Otto, R.; Xie, J.; Brox, J.; Trippel, S.; Stei, M.; Best, T.; Siebert, M. R.; Hase, W. L.; Westen, R. *Faraday Discuss. Chem. Soc.* **2012**, *157*, 41-57
12. Zhang, J.; Hase, W. L. *J. Phys. Chem. A.* **2010**, *114*, 9635-9643
13. Aikens, C. M.; Webb, S. P.; Bell, R. L.; Fletcher, G. D.; Schmidt, M. W.; Gordon, M. S. *Theoret. Chem. Acc*. **2003**, *110*, 233-253
14. Parr, R. G.; Weitao, Y. Density-Functional Theory of Atoms and Molecules (Oxford University Press, USA, 1994).
15. Perdew, J. P.; Burke, K.; Ernzerhof, M. *Phys. Rev. Lett.* **1996**, *77*, 3865-3868
16. Lee, C.; Yang, W.; Parr, R. G. *Phys.Rev.* **1988**, *37*, 785-789
17. Hamprecht, F. A.; Cohen, A.; Tozer, D. J.; Handy, N. C. *J. Chem. Phys.* **1998**, *109*, 6264-6271.
18. Becke, A. D. *J. Chem. Phys.* **1993**, *98*, 1372-1377.
19. Zhang, J.; Mikosch, J.; Trippel, S.; Otto, R., Weidemuller; M.; Wester; R., Hase, W. L. *J. Phys. Chem. Lett.* **2010**, *1*, 2747-2752
20. Mikosch, J.; Zhang, J.; Trippel, S.; Eichhorn C.; Otto, R.; Sun, R.; de Jong, W. A.; Weidemuller; M.; Hase, W. L.; Wester; R. *J. Am. Chem. Soc.* **2013**, *135*, 4250-4259

21. Sun, R.; Xie, J; Zhang, J.; Hase, W. L. *Int. J. Mass Spectrom.*, doi:http://dx.doi.org/10.1016/j.ijms.2014.04.006
22. Raghavachari, K.; Trucks, G. W.; Pople, J. A.; Head-Gordon, M. *Chem. Phys. Lett.* **1989**, *157*, 479-483
23. Wadt, W. R.; Hay, P. J. *J. Phys. Chem.* **1985**, *82*, 284-298
24. Dunning, T. H., Jr. *J. Chem. Phys.* **1989**, *90*, 1007-1023
25. Woon, D. E.; and Dunning, T. H., Jr. *J. Chem. Phys.* **1993**, *98*, 1358-1371
26. Hu, W. P.; Truhlar, D. G. *J .Phys. Chem.* **1994**, *98*, 1049-1952
27. Peterson, K. A.; Shepler, B. C.; Figgen, D.; Stoll, H. *J. Phys. Chem. A* **2006**, *110*, 13877-13883.
28. Fukui, K. *Acc. Chem. Res.* **1981**, *14*, 363-368
29. D. L. Bunker, *J. Chem. Phys.* **1962**, *37*, 393-403
30. Sun, R.; Park, K.; de Jong, W. A.; Lischka, H.; Windus. T. L.; Hase, W. L. *J. Chem. Phys.* **2012**, *137*, 044305
31. Yang, L.; Sun, R.; Hase, W. L. *J. Chem. Theory Comput.* **2011**, *7*, 3478-3483
32. Hase, W. L. *J. Phys. Chem.* **1986**, *90*, 365-374
33. Lourderaj, U.; Park, K.; Hase, W. L. *Int. Rev. Phys. Chem.* **2008**, *27*, 361-403
34. Sun, L.; Hase, W. L. *Rev. Comput. Chem.* **2003**, *19*, 79-146
35. Paranjothy, M.; Sun, R.; Zhuang, Y.; Hase, W. L. *WIREs Comput. Mol. Sci.* **2013**, *3*, 296-316
36. Szalbo, A and Ostlund, N. S. *Modern Quantum Chemistry, Introduction to Advanced Electronic Structure Theory* (Dover, New York, **1996**)
37. Lourderaj, U.; Sun, R.; Swapnil, C. K.; Barnes, G. L.; de Jong, W. A.; Windus, T. L.; Hase, W. L. *Comput. Phys. Commun.* **2014**, *185*, 1074–1080
38. Hase, W. L.; Duchovic, R. J.; Hu, X.; Komornicki, A.; Lim, K. F.; Lu, D. H.; Peslherbe, G. H.; Swamy, S. R.; Vande Linde, S. R.; Varandas, A. *et al.*, *QCPE Bull.* **1996***, 16,* 671
39. Hu, X.; Hase, W. L.; Pirraglia, T. *J. Comput. Chem.* **1991**, *12*, 1014-1024
40. Valiev, M.; Bylaska, E. J.; Govind, N.; Kowalski, K.; Straatsma, T. P.; van Dam, H. J. J.; Wang, D.; Nieplocha, J.; Apra, E.; Windus, T. L.; de Jong, W. A. *Comput. Phys. Commun.* **2010**, *181*, 1477-1489
41. Schlick, T. *Molecular Modeling and Simulation* (Springer, New York, 2000)
42. Peslherbe, G. H.; Wang, H.; Hase, W. L. *Adv. Chem. Phys.* **1995**, *105*, 171-202

43. Sun, L.; Hase, W. L.; Song, K. *J. Am. Chem. Soc.* **2001**, *123*, 5753-5756.
44. Miller, W. H.; Hase, W. L.; Darling, C. L. *J. Chem. Phys.* **1989**, *91*, 2863-2868.
45. Swamy, K. N.; Hase, W. L. *J. Phys. Chem.* **1983**, *87*, 4715-4720.
46. Schatz, G.C. *J. Chem. Phys.* **1983**, *79*, 5386-5391.
47. Hase, W. L.; Buckowski, D. G. *J. Comput. Chem.* **1982**, *3*, 335-343.
48. Lu, D.; Hase, W. L. *J. Chem. Phys.* **1988**, *89*, 6723-6736.
49. Zhang, J.; Lourderaj, U.; Sun, R.; Mikosch. J.; Wester, R.; Hase, W. L. *J. Chem. Phys.* **2013**, *138*, 114309.
50. Mikosch, J.; Trippel, S.; Eichhorn, C.; Otto, R.; Lourderaj, U.; Zhang, J.; Hase, W. L.; Weidemüller, M.; Wester, R. *Science* **2008**, *319*, 183-186
51. Y. J. Cho, S. R. Vande Linde, L. Zhu and W. L. Hase, *J. Chem. Phys.* **1992**, *96*, 8275-8287.
52. Lu, D.; Hase, W. L. *J. Chem. Phys.* **1989**, *91*, 7490-7497.
53. Xie, J.; Kohale, S. C.; Hase, W. L.; Ard, S. G.; Melko, J. J.; Shuman, N. S.; Viggiano, A. A. *J. Phys. Chem. A* **2013**, *117*, 14019-14027.

Table 1. Average Fractions of $F^- + CH_3I \rightarrow CH_3F + I^-$ Product Energy Partitioning

	f_{rot}	f_{vib}	f_{rel}	f_{int}
		DFT/B97-1[b]		
direct rebound	0.19 ± 0.03	0.27 ± 0.04	0.54 ± 0.03	0.46 ± 0.03
direct stripping	0.27 ± 0.03	0.45 ± 0.04	0.28 ± 0.02	0.72 ± 0.02
indirect	0.07 ± 0.03	0.62 ± 0.04	0.31 ± 0.02	0.69 ± 0.02
total	0.12 ± 0.03	0.51 ± 0.06	0.37 ± 0.04	0.63 ± 0.04
		MP2		
direct rebound	0.07 ± 0.01	0.56 ± 0.02	0.37 ± 0.02	0.63 ± 0.02
direct stripping	0.21 ± 0.02	0.45 ± 0.01	0.34 ± 0.01	0.66 ± 0.02
indirect	0.14 ± 0.05	0.71 ± 0.07	0.15 ± 0.03	0.85 ± 0.07
total	0.13 ± 0.01	0.53 ± 0.01	0.34 ± 0.01	0.66 ± 0.01
		Experiment [b]		
total				0.59 ± 0.08

a. The *f's* are fractions of energy partitioned to rotational, vibrational, relative translational, and internal (rotation + vibration) energy. Total is the combined partitioning for the mechanisms.

b. Data obtained from Table 2 of reference 20.

Figure Captions

Figure 1. Critical points on the potential energy surface for the $F^- + CH_3I \rightarrow FCH_3 + I^-$ S_N2 reaction: (a) CCSD(T)/PP/t (black), MP2/ECP/d (red), and experiment (blue); (b) DFT/B97-1 (black) and experiment (blue). The potential energies (kJ/mol) are classical energies without zero point energy. The DFT/B97-1 results were presented previously.[19,20]

Figure 2. Reaction probabilities, $P_r(b)$, for the $F^- + CH_3I$ S_N2 reaction versus impact parameter: MP2 dynamics top graph and DFT/B97-1 dynamics bottom graph. The lines are for the total S_N2 (blue solid line with circle), direct rebound (black dash line with upper triangle), direct stripping (red dash line with down triangle), and indirect (green dash line with square) reactions. The DFT/B97-1 results were presented previously.[19,20]

Figure 3. Normalized histogram distributions of the CH_3F internal (rotation + vibration) energy for the MP2 and B97-1 simulations. The black solid curve is the experimental result and the blue dash curve is from simulation. The DFT/B97-1 results were presented previously.[19,20]

Figure 4. Normalized histogram distributions of the velocity scattering angle distribution for the $F^- + CH_3I \rightarrow FCH_3 + I^-$ S_N2 reaction. The results for both the MP2 and B97-1 simulations are presented in the blue dash curves. The black solid curve is the experimental result. Negative and positive cos(θ) correspond to backward and forward scattering, respectively. The DFT/B97-1 results were presented previously.[19,20]

Figure 5. Velocity scattering angle distributions from MP2(blue dash) and B97-1(red solid) for the rebound, stripping, and indirect mechanisms. The sum of the individual distributions is normalized to unity. The area of each distribution is proportional to its contribution to the atomistic dynamics. The DFT/B97-1 results were presented previously.[19,20]

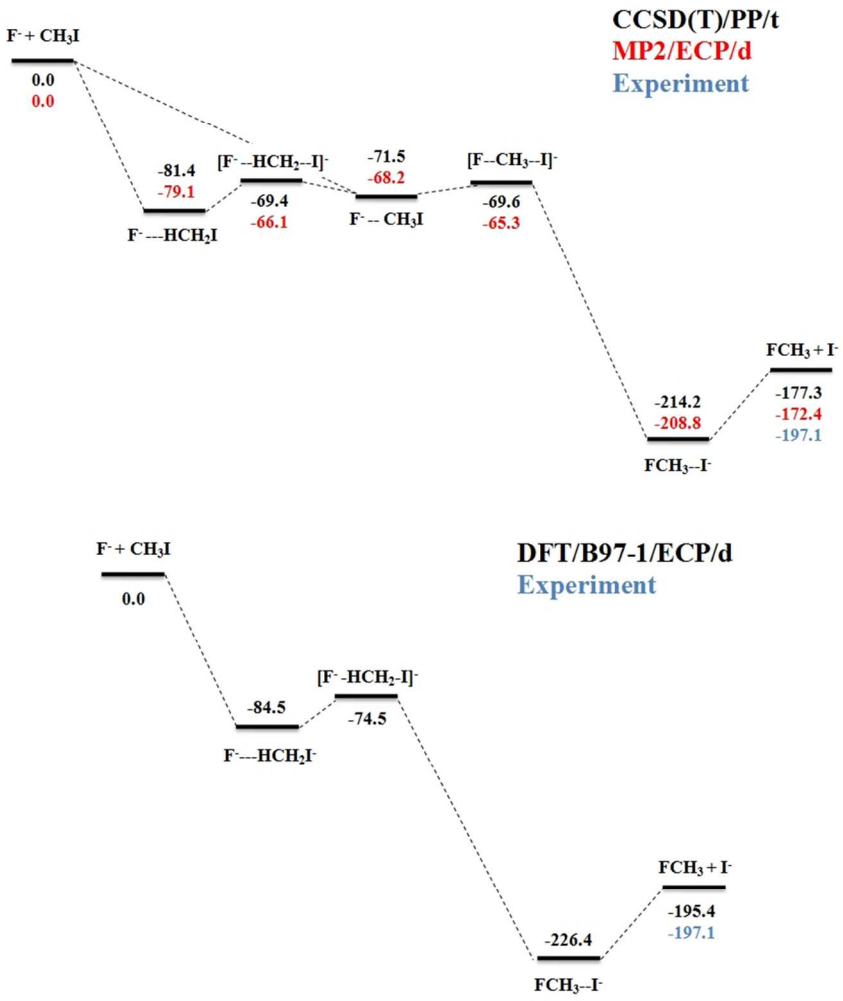

Figure 1

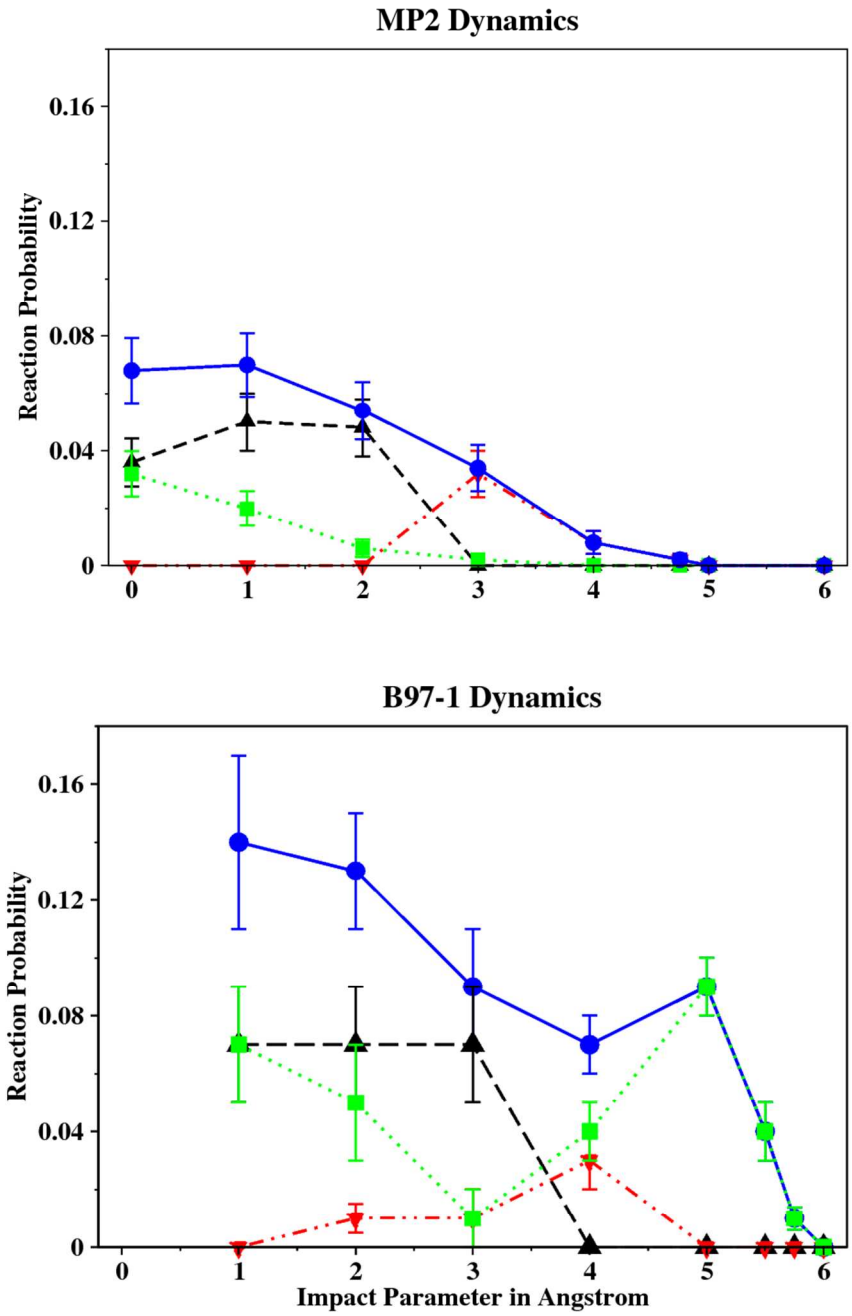

Figure 2

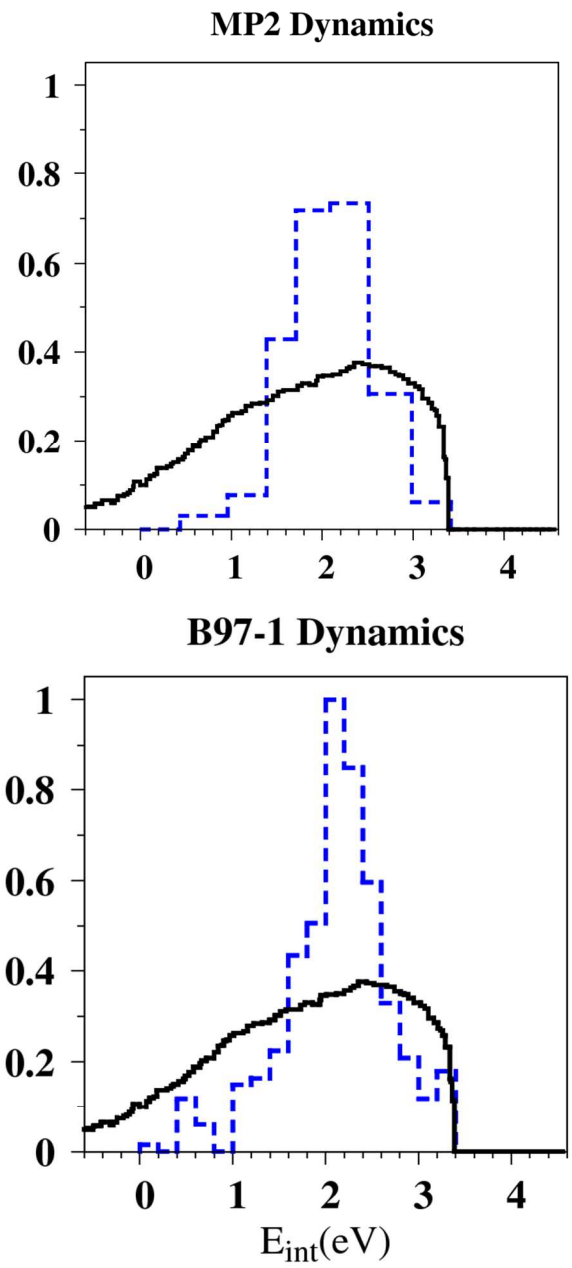

Figure 3

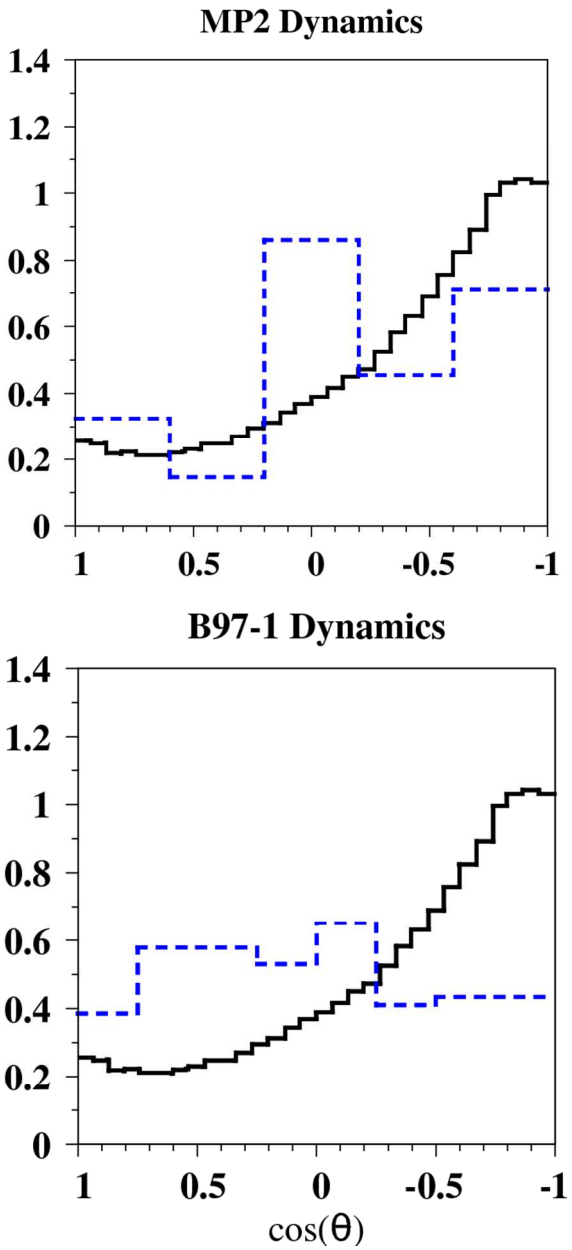

Figure 4

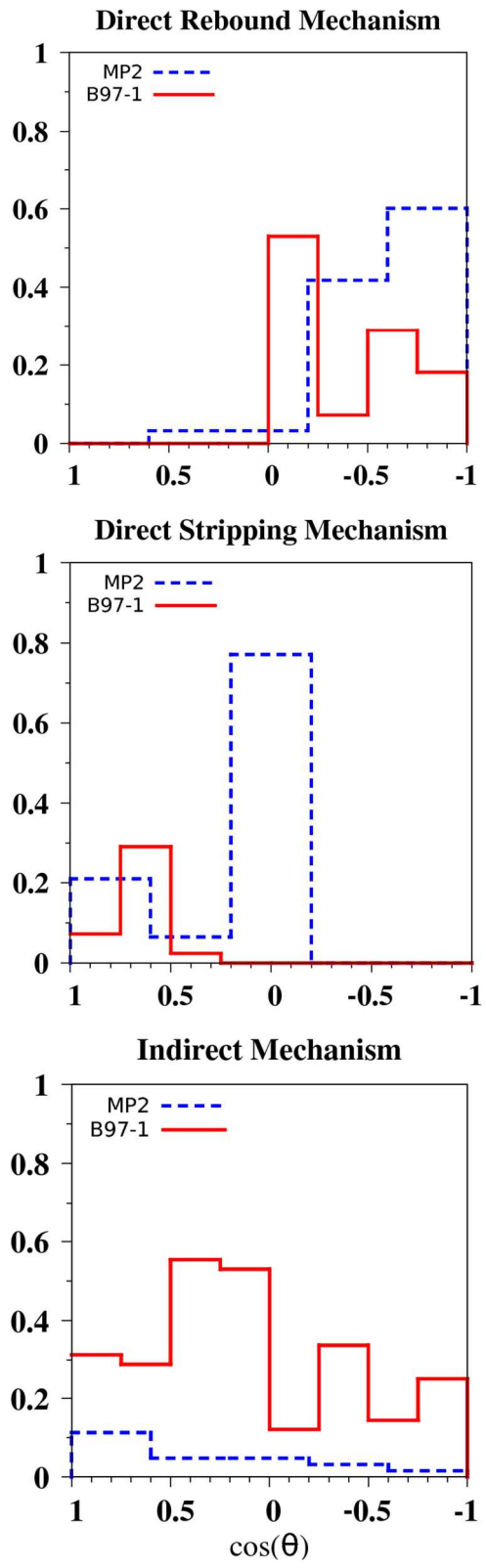

Figure 5